Journal of Catalysis **182,** 367–377 (1999)
Article ID jcat.1998.2361, available online at http://www.idealibrary.com on IDEAL®

Spectroscopic Study of a Cu/CeO_2 Catalyst Subjected to Redox Treatments in Carbon Monoxide and Oxygen

A. Martínez-Arias,[1] M. Fernández-García, J. Soria, and J. C. Conesa

Instituto de Catálisis y Petroleoquímica, CSIC, Campus Universitario de Cantoblanco, Camino de Valdelatas s/n, 28049 Madrid, Spain

Received July 8, 1998; revised November 17, 1998; accepted November 19, 1998

Redox processes induced by interaction of a calcined Cu/CeO_2 catalyst with CO and reoxidation with O_2 have been investigated by CO-TPR, EPR, FTIR of adsorbed CO, and XPS. The initial calcined sample shows the presence of dispersed Cu^{2+} species, which give rise in the EPR spectrum to signals due to isolated entities, a somewhat more aggregated Cu^{2+}-containing phase, and copper ionic pairs, in coexistence with an EPR-silent CuO-type phase, revealed by XPS. A significant reduction of copper is produced already by contact with CO at room temperature, EPR results suggesting that reducibility of Cu^{2+} species decreases with their aggregation degree. Simultaneously, the ceria surface is also reduced by this interaction, copper acting as a strong promoter of this process. A singular consequence of the synergistic reduction of both components is observed by subjecting the catalyst to CO at $T_r \geq 473$ K, at which the CO adsorption capability of copper is apparently suppressed, in view of the absence of copper carbonyls in the FTIR spectrum. This is attributed to the establishment of electronic interactions between reduced ceria and small metallic copper particles generated by the reduction process. Contact of the CO-reduced sample with O_2 at room or higher temperature produces an important reoxidation of both copper and ceria, revealed by FTIR and EPR. The synergetic effects between copper and ceria in the reduction process and the easy reoxidation of deeply reduced ceria are thought to be crucial to explaining the high catalytic activity shown by this system for CO oxidation.

INTRODUCTION

Cerium oxide is widely used as a promoter in the so-called "three-way catalysts" for the elimination of toxic exhaust gases in automobiles (1). The promoting effect of cerium oxide was originally attributed to the enhancement of the metal dispersion and the stabilization of the support towards thermal sintering (2). It was later shown that ceria can also act as a chemically active component, working as an oxygen store by release of oxygen in the presence of reductive gases and removal of it by interaction with oxidizing gases (3), and participating in the water–gas shift reaction (4) or the decomposition of nitrogen oxides (5). More recent efforts are devoted to elucidating the participation of ceria in important metal/ceria interactions induced by the establishment of contacts between both components, which strongly affect their redox and, as a consequence, catalytic properties (6–8).

In the case of systems containing both copper and cerium oxide, the formation of intimate contacts between both components is thought to be of crucial importance in explaining the remarkably high activities exhibited by Cu/CeO_2 catalysts for methanol synthesis (9) or for carbon monoxide oxidation (10, 11). In this latter reaction, previous works have shown an important promoting effect upon ceria addition to the catalysts, leading to significant decreases of the isoconversion temperatures, with respect to more conventional alumina-supported copper (11, 12) or unsupported copper oxide (10, 13). This promoting effect was proposed to be due to both redox state promotion and bifunctional promotion (10, 11). Thus, a synergistic reaction model to explain the enhanced catalytic activity shown by Cu–Ce binary oxides has been proposed, in which Cu^+ species stabilized by interactions between copper oxide clusters and cerium oxide provide surface sites for CO adsorption while the cerium oxide provides the oxygen source (10). Our previous work on CO oxidation catalytic activity over $Cu/CeO_2/Al_2O_3$ catalysts attributed an important role, in relation to the reactivity promotion, to the formation of contacts between copper and relatively large three-dimensional ceria crystals (so-called 3D-Ce entities) (11). More recently, it has been shown that these particular copper entities show an important redox activity upon interactions with carbon monoxide, FTIR of adsorbed CO showing an easy generation of metallic copper by contact with CO at relatively low reduction temperatures (14). This easier reduction of copper interacting with 3D-Ce is presumed to favor the catalytic activity for CO oxidation, not only because the activity of copper increases with its reduction degree (15), but also because metal–support interactions would be activated. In order to clarify these aspects, in this contribution we have examined a Cu/CeO_2 catalyst which, as reported in a previous work (11), shows a relatively high

[1] To whom correspondence should be addressed. E-mail: amartinez@icp.csic.es.

0021-9517/99 $30.00

activity for CO oxidation: 20% conversion at room temperature (RT, ca. 298 K) and 100% conversion at 398 K, using a stoichiometric 1% CO + 0.5% O_2 in N_2 reactant mixture at 30,000 h^{-1} space velocity; our attention is here focused on the analysis of its redox behavior upon interactions with CO and oxygen.

EXPERIMENTAL

Materials

A high surface area CeO_2 sample (supplied by Rhône-Poulenc, $S_{BET} = 287\ m^2\,g^{-1}$) was used as support. The Cu/CeO_2 catalyst (to a final copper load of 1 wt%, representing ca. 157 μmol of Cu per gram of catalyst) was prepared by impregnation of the CeO_2 support with an aqueous solution of $Cu(NO_3)_2 \cdot 3H_2O$ (Merck, 99.5% purity). The resulting material was dried overnight at 353 K and subsequently calcined at 773 K under a dry air flow for 4 h. After this pretreatment, the sample showed a surface area $S_{BET} = 260\ m^2\,g^{-1}$. Preliminary characterization experiments on this Cu/CeO_2 sample, performed by XRD (results not shown), showed only peaks due to the ceria fluorite structure of similar characteristics for both the CeO_2 support and the Cu/CeO_2 sample.

All the employed gases were of commercial purity and, for adsorption experiments, were further purified, before storage, by vacuum distillation methods.

Techniques

EPR spectra were recorded at 77 K with a Bruker ER 200 D spectrometer operating in the X-band and calibrated with a DPPH standard ($g = 2.0036$). Portions of about 50 mg of sample were placed inside a quartz probe cell with greaseless stopcocks using a conventional high vacuum line (capable of maintaining a dynamic vacuum of ca. 0.006 $N\,m^{-2}$) for the different treatments. Except where specified, CO reduction treatments at a specific reduction temperature (T_r) were made under static conditions using 100 Torr of CO, heating during 1 h at the corresponding T_r and subsequently outgassing at the same temperature for 0.5 h.

FTIR spectra were recorded at RT with a Nicolet 5ZDX Fourier Transform spectrometer, with a resolution of 4 cm^{-1}, 128 scans per spectrum, and subtracting the gas-phase contribution in all cases. Thin self-supporting discs (ca. 20 $mg\,cm^{-2}$) were prepared by pressing the powders at 2500 $N\,cm^{-2}$ and were handled in standard greaseless cells, where they could be subjected to thermal or adsorption treatments. Reduction treatments in CO similar to those described above for EPR were carried out for the FTIR experiments.

For the CO-TPR experiments, 5 g of sample was placed in a quartz flow reactor. After a standard precalcination treatment consisting of heating under a 3% O_2:N_2 flow at 673 K for 1 h, cooling in the same gas flow to RT, and then purging briefly (5 min) with N_2, the mixture is switched to a 1% CO/N_2 mixture, using a rate of 200 $cm^3\,min^{-1}$ (thus supplying ca. 82 μmol CO min^{-1}) and, after a short time (ca. 3 min, enough to stabilize outlet gas composition in the absence of reaction), a programmed temperature ramp is initiated at a rate of 5 $K\,min^{-1}$ from RT up to 773 K, with the evolved gases being monitored every 5 K. The analysis of the feed and outlet gas streams was performed using a Perkin–Elmer FTIR spectrometer mod. 1725X, coupled to a multiple reflection transmission cell (Infrared Analysis, Inc., "long path gas minicell," 2.4 m path length, ca. 130 cm^3 internal volume).

Photoelectron spectra were acquired with a VG ESCALAB 200R spectrometer equipped with a hemispherical electron analyzer and a Mg$K\alpha$ 120 W X-ray source. A PDP 11/04 computer from Digital Equipment Co. was used for collecting and analyzing the spectra. The powder samples were pressed into small aluminum cylinders and then mounted on a sample rod placed in an *in situ* pretreatment chamber and heated under vacuum at RT for 1 h prior to being moved into the analysis chamber adjacent to the pretreatment one. The pressure in the ion-pumped analysis chamber was maintained below 3×10^{-9} Torr (1 Torr = 133.33 $N\,m^{-2}$) during data acquisition. Spectra were collected for 20 to 90 min, depending on the peak intensities, using low X-ray fluxes (60–120 W) to minimize photoreduction of the sample, at a pass energy of 20 eV (1 eV = 1602×10^{-19} J), which is typical of high-resolution conditions. The intensities were estimated by calculating the integral of each peak after subtraction of the "S-shaped" background and using experimental factors affecting quantitative data, viz. ionization cross section, electron escape depth, and instrumental sensitivity. All binding energies (BE) were referenced to the adventitious C 1*s* line at 284.9 eV. This reference gave BE values within an accuracy of ± 0.2 eV.

RESULTS AND ASSIGNMENT OF SPECTRAL FEATURES

CO-TPR

Figure 1 shows the profiles obtained in the CO-TPR experiment from RT up to 773 K for Cu/CeO_2. The profile shows CO consumption features at RT (which suggests that a specific maximum would appear below RT, if the TPR starting temperature were been lower), and 478 and 518 K. Although precise quantification of the amount of CO consumed in the first peak ($T < 340$ K) is not possible, due to the fact that the experiment is started after a certain equilibration time (see Experimental), a lower limit of this value can be obtained by integration: ca. 42 μmol CO per gram of catalyst. Around 291 μmol CO per gram of catalyst is estimated to be consumed between 340 and 773 K. However, CO_2 does not evolve in a parallel way for $T <$ ca. 473 K; it first appears at 443 K and shows a maximum at 518 K,

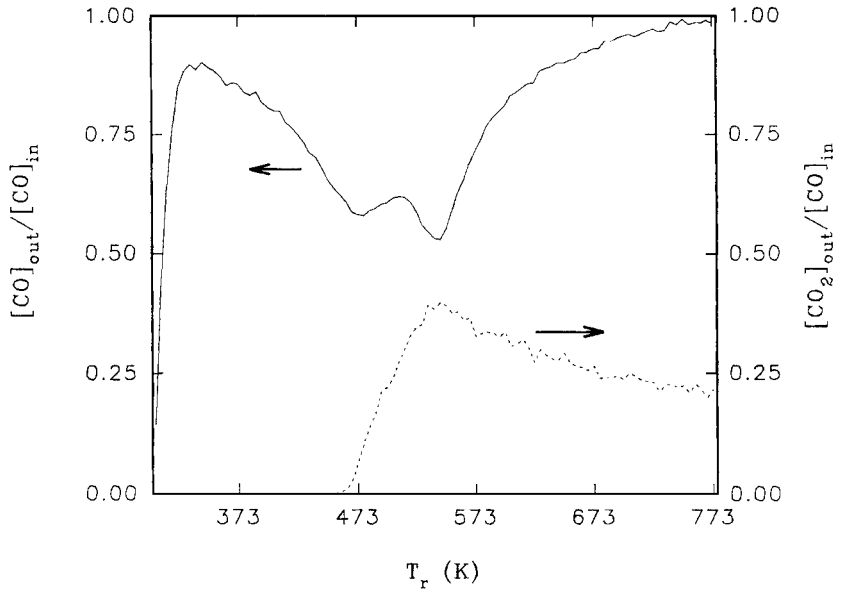

FIG. 1. CO-TPR profiles of Cu/CeO_2 (solid line, CO; dashed line, CO_2).

in coincidence with the high-temperature maximum of CO consumption. The noncoincidence of the lower temperature peaks of CO consumption and CO_2 production, and the presence of a CO_2 evolution tail at high T_r, suggest that adsorption–desorption phenomena are involved to a certain degree in the profiles obtained.

EPR

Initial calcined sample. Figure 2a shows the EPR spectrum of the initial sample, obtained after calcination pretreatment in O_2 of Cu/CeO_2 at 773 K. Only 25% of the total copper content is detected in this spectrum (as concluded comparing the integrated intensity with that of a copper sulfate standard). Spectral analysis of the different peaks observed and of the different evolution of the signals upon redox treatments has allowed us to discern the contribution of different signals to this complex spectrum (Table 1 gives a summary of the parameters of these signals). The most prominent signals present a lineshape characteristic of species with an axial (or near axial) symmetry with $g_\parallel > g_\perp > g_e$ and four-line hyperfine splittings due to the interaction of the unpaired electrons with nuclei of spin $I = 3/2$ (signal type C), the major contribution to the spectrum of Fig. 2a being due to signals C1 and C2 while another signal of this kind, C3, is contributing in a lower extent. The spectrum also shows the presence of a doublet centered at $g = 2.040$ and separated by ca. 650 G, signal K, and another broad and poorly resolved signal B centered around $g = 2.11$.

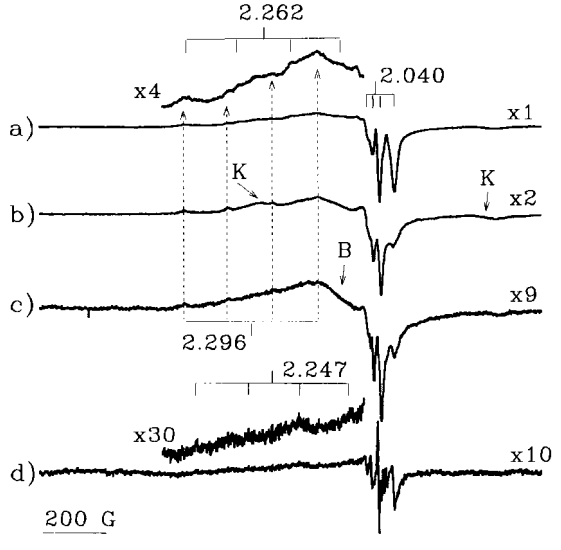

FIG. 2. EPR spectra of Cu/CeO_2. (a) Initial calcined sample. (b) Following admission of 280 μmol g^{-1} of CO at 77 K and warming at RT. After reduction treatment in CO at (c) $T_r = 373$ K and (d) $T_r = 473$ K. (Note the enlarged $g_\parallel$ parts of (a) and (d) are also shown.)

TABLE 1

EPR Parameters of the Signals Due to Cu^{2+} Ions Observed in This Work for Cu/CeO_2 (Parameters of Type C Signals Were Obtained by Computer Simulations)

Signal	$g_\parallel$	$g_\perp$	$A_\parallel$ (cm^{-1})	$A_\perp$(cm^{-1})
C1	2.296	2.035	14.5×10^{-3}	1.90×10^{-3}
C2	2.262	2.040	16.2×10^{-3}	2.85×10^{-3}
C3	2.247	2.036	16.3×10^{-3}	1.78×10^{-3}
B	$\langle g \rangle = 2.11$			
K		2.040		

Reduction treatments in CO. No particular change is observed in the spectrum of the calcined sample upon adsorption of a small amount of CO (280 μmol per gram of catalyst) at 77 K. However, upon subsequent warming at RT for 30 min (Fig. 2b), an important decrease of the overall intensity is produced, signal C2 being affected the most by this treatment. A further decrease of the overall intensity is produced by CO reduction treatments at higher temperature. Thus, treatment at $T_r = 373$ K (Fig. 2c) produces an important decrease of all the signals observed in the initial spectrum. Signals C2, C1, and K seem particularly affected by this interaction, while the higher relative contribution of signal B indicates the higher resistance of these centers to this treatment. For $T_r = 473$ K (Fig. 2d), only the presence of a weak signal C3 can be discerned. The Cu^{2+}/Cu_{tot} (%) ratios were 25 for the calcined catalyst and 15, 5, 1.25, and 1 after subsequent treatments with CO at RT, and 373, 473, and 573 K, respectively.

Assignment of copper signals. Type C signals are typical of isolated Cu^{2+} ions, their different EPR parameters reflecting differences in the coordination environments of the corresponding ions (16). Their g and A anisotropic tensor values can be correlated with Cu^{2+} ions located, in general terms, at tetragonally distorted octahedral sites; shifts of $g_\parallel$ to lower values and of $A_\parallel$ to higher values indicate increases in the tetragonal distortion (axial lengthening and planar shortening), which might be caused by coordination changes from a pure tetragonally distorted octahedral coordination to square pyramidal and, further, to square planar coordinations (17). The relatively high reactivity towards CO shown by signal C1 and, most particularly, signal C2, and the observation of another type C signal (with higher $g_\parallel$ and lower $A_\parallel$ than signal C1, and unresolved $A_\perp$) that can be assigned to hexa-coordinated Cu^{2+}, for another Cu/CeO_2 sample (presumably presenting a higher hydroxylation degree since it was merely outgassed at RT after the drying step of the preparation) (16), suggest that the species corresponding to signals C1 and C2 could present some degree of coordinative unsaturation, which leads us to tentatively assign them to Cu^{2+} in, respectively, square pyramidal and square planar sites. Signal C3 might also be attributed to Cu^{2+} ions with square planar coordination, although in view of their lower reactivity towards CO, they are probably not directly exposed at the sample surface but rather located at ceria subsurface positions; actually, a signal showing parameters close to those observed here for signal C3 has been proposed to be due to Cu^{2+} in substitutional sites of the ThO_2 lattice in Cu-doped thoria samples (18).

Signal B, showing an average $\langle g \rangle$ value similar to those of type C signals, must be due to Cu^{2+} ions as well; its larger linewidth (and consequently its unresolved hyperfine splitting) might be attributed to dipolar broadening effects produced by mutual interactions between paramagnetic Cu^{2+} ions, suggesting that the corresponding ions are located in a Cu^{2+}-containing aggregated phase (probably Cu oxide clusters). Signal K is similar to that reported previously (16) and corresponding to Cu^{2+} ion pairs, formed by two equivalent ions in an axial symmetry. In this case, only the fine-structure twofold splitting of the perpendicular component of the signal can be resolved, yielding two peaks with separation $\Delta H = 650$ G. This poorer resolution and the modification of the signal upon relatively mild adsorption treatments (as shown later) suggest that the corresponding Cu^{2+} ion pairs are located at surface or near-surface zones of the catalyst, where they can be affected by nonhomogeneous environments leading to line broadening effects. This contrasts with previous works (16), in which $Cu–CeO_2$ samples were prepared by coprecipitation and/or submitted to more severe redox treatments, with the consequence that the copper ions probably diffused to more homogeneous positions in the ceria bulk, leading to a much better resolved signal K and to detection of hyperfine splittings which showed the participation of two Cu nuclei in the species originating it.

Interaction of CO-reduced Cu/CeO_2 with O_2. Adsorption of a small amount of O_2, 56 μmol per gram of catalyst (μmol g^{-1}), at 77 K (followed by outgassing at 77 K) on Cu/CeO_2 previously reduced in CO at $T_r =$ RT, and 373 and 473 K produces the appearance of new sharp features in spectrum positions close to $g = 2.0$, indicating the formation of adsorbed oxygen radicals (type O signals), whose intensity decreases with increasing T_r. After performing a subtraction operation, in order to cancel Cu^{2+} signal contributions, the formation of an orthorhombic signal O1, with $g_z = 2.031$, $g_x = 2.015$, and $g_y = 2.010$ (axes assignment of the g tensor parameters being made according to conventions of previous works (19, 20)), can be discerned for $T_r =$

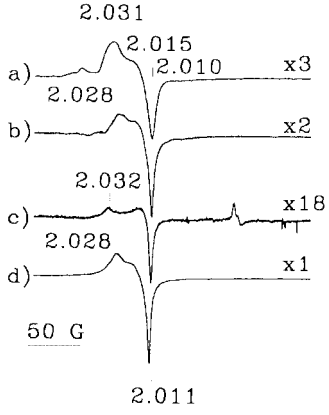

FIG. 3. EPR spectra of Cu/CeO_2 (a, b) and CeO_2 (c, d) after adsorbing an amount Q of oxygen at 77 K on the samples reduced in CO at temperature T_r. (a) $Q = 56$ μmol g^{-1}, $T_r =$ RT. (b) $Q = 280$ μmol g^{-1}, $T_r = 473$ K. (c) $Q = 56$ μmol g^{-1}, $T_r = 473$ K. (d) $Q = 168$ μmol g^{-1}, $T_r = 573$ K. (For (a) and (b), spectra subtraction operations have been done in order to cancel contributions of Cu^{2+} signals.)

RT or 373 K (Fig. 3a). For $T_r = 473$ K, it is not possible to determine accurately the parameters of the signals formed due to their low intensity. Subsequent warming at RT of the sample with O_2 adsorbed at 77 K leads in all cases (T_r = RT–473 K) to a strong decrease (or disappearance) of the type O signals, along with certain increase of the signals due to Cu^{2+} species.

These reoxidation processes have been investigated in more detail for the sample reduced at $T_r = 473$ K, by following an adsorption cycle consisting in: (a) adsorption of a certain known dose of O_2 at 77 K (in this case without outgassing at 77 K); (b) subsequent warming at RT; and (c) repetition of steps (a) and (b) (dose of O_2 at 77 K + warming at RT) several times, thus gradually increasing the amount of O_2 introduced into the cell.

Considering exclusively the spectra obtained after step (a) of the adsorption cycle, it is observed that upon increasing the amount of oxygen admitted in the cell up to a cumulative amount of 280 μmol g^{-1}, an increase in the intensity of type O signals is produced, the maximum in the first-derivative spectra (feature around $g = 2.03$) being somewhat shifted to lower g values with respect to signal O1 (a characteristic spectrum obtained in these conditions is shown in Fig. 3b). This reveals the formation of new type O signals with parameters $g_z = 2.029$–2.027, $g_x = 2.016$–2.015, and $g_y = 2.011$ (generically referred to as O2 signals). A small amplitude decrease of type O signals, along with a noticeable broadening of them is observed when the amount of O_2 is increased to 560 μmol g^{-1} of O_2, this effect being more pronounced when the amount adsorbed raises to 840 μmol g^{-1}; this is most likely due to magnetic dipolar interactions between paramagnetic nonchemisorbed O_2 and the superoxide species giving rise to type O signals, following saturation of the oxygen adsorption centers.

The behavior of type O signals after step (b) of the adsorption cycle depends on the cumulative amount of oxygen previously admitted in the cell. Thus, for amounts up to 280 μmol g^{-1}, a fast decrease of the signals is produced upon RT warming, only 2 min warming leading to their almost complete disappearance. However, when 560 μmol g^{-1} has been admitted, no important change (only a small increase) in the intensity of the type O signals is produced after 2 min warming, and a small signal O2 is still detected even after 3 h warming at RT.

The evolution of signals due to Cu^{2+}-related species upon increasing the amount of O_2 admitted in the cell at RT (step (b)) is shown in Figs. 4a–4c. This reveals first the growth of mainly signal C3 for a low O_2 dose (Fig. 4b), while signals B and K increase as well when a higher O_2 dose is admitted (Fig. 4c). No important changes are observed upon heating the sample in O_2 at 373 K. However, heating in O_2 at 473 K produces a certain increase of signals C1 and C2, while the overall intensity is somewhat increased by heating at 573 K, mainly because of the increase of signals C1 and C2 (Fig. 4e). A complete recovery of the

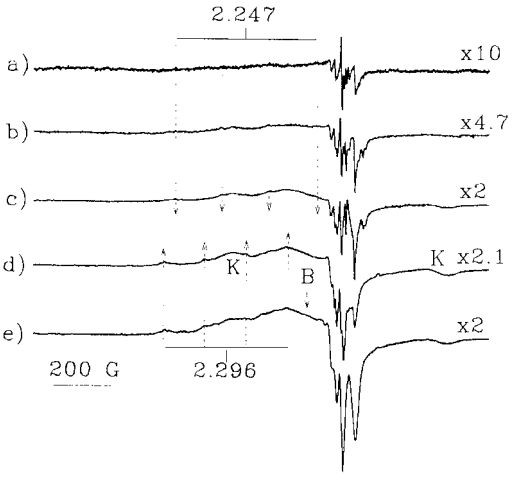

FIG. 4. EPR spectra of Cu/CeO_2. (a) Reduced in CO at $T_r = 473$ K. Subsequent adsorption of (b) 280 μmol g^{-1} and (c) 560 μmol g^{-1} of O_2 at RT. Further heating in 100 Torr of O_2 at (d) 473 K and (e) 573 K.

overall intensity of the initial calcined sample (spectrum shown in Fig. 2a) is not achieved by these reoxidation treatments, its extent being roughly of 20% at RT and 60% at 573 K.

Unlike in the case of Cu/CeO_2, no type O signal is detected upon adsorption of O_2 at 77 K or RT on the Cu-free CeO_2 support reduced at T_r = RT, while only a very weak and unresolved signal type O, recognized by a sharp feature at $g \approx 2.011$, is produced when $T_r = 373$ K. A more intense signal O1 with $g_z = 2.032$, $g_x = 2.013$, and $g_y = 2.010$ is produced by O_2 adsorption at 77 K on CeO_2 reduced in CO at $T_r = 473$ K (Fig. 3c), whose intensity slightly increases upon warming at RT. Phenomena similar to those observed in Cu/CeO_2 treated in CO at $T_r \geq$ RT, involving formation of type O signals upon O_2 adsorption at 77 K and their decrease (or disappearance) upon warming at room temperature, can be also observed for CeO_2, but at a significantly higher prereduction T_r ($T_r = 573$ K) than for Cu/CeO_2 (T_r = RT). When a similar O_2 adsorption cycle (involving adsorption of cumulative amounts of O_2) is followed over CeO_2 reduced at $T_r = 573$ K, the intensity of the type O signals registered after each dosing at 77 K (step (a) of the adsorption cycle) increases with the amount of oxygen admitted, reaching a maximum for a total O_2 dose of ca. 168 μmol g^{-1}; a slight amplitude decrease along with certain broadening of the signals is produced for larger doses. In a way similar to Cu/CeO_2, the shape of the spectra changes with the amount of oxygen admitted in the cell, the maximum in the first-derivative spectra being shifted from 2.030 to 2.028, when the O_2 dose is increased from 56 to 168 μmol g^{-1}. A typical spectrum obtained under these conditions is shown in Fig. 3d. This shows, as in the case of Cu/CeO_2, the appearance of signals O2, rather than O1, upon increasing the amount of oxygen adsorbed at 77 K. Warming for 30 min at RT (step (b) of the adsorption cycle)

leads to the disappearance of the type O signals, except when 224 μmol g^{-1} has been admitted, in which case, although an important decrease of the signals occurs, a small signal O2 still remains.

Assignment of type O signals. Based on previous studies of oxygen adsorption on pure ceria (19) or supported ceria materials (20) type O signals can be attributed to superoxide species adsorbed on cerium ions (formally O_2^-–Ce^{4+}). While signal O1 is similar to one of the signals found in pure ceria (19), the parameters of signal O2 do not coincide with any of the signals observed in that material submitted merely to outgassing pretreatments; rather, they are similar to those O_2^-–Ce^{4+} formed, by O_2 adsorption on outgassed samples, in dispersed ceria systems (20, 21) or in pure ceria samples in which the oxygen adsorption centers are coordinatively modified by the presence of residual chloride ions (21, 22). The differences in the EPR parameters of signal O2, with respect to the superoxide species observed on unmodified outgassed pure ceria, are certainly due to changes in the environments of the corresponding superoxide species, producing variations in the electrostatic or polarization effects affecting the paramagnetic centers. These changes might thus be attributed to the modifications of the ceria surface produced by the presence of copper ions and/or of adsorbed species generated either by prior CO interaction (carbonate-type or carbonaceous species) or by the oxygen adsorption itself (formation of superoxide or peroxide species). Since similar signals are observed after CO reduction in both CeO_2 and Cu/CeO_2 (thus discarding important copper specific effects), and there seems to be no evidence of these signals in pure CeO_2 samples strongly reduced in H_2 (23) (thus discarding effects due to chemisorbed oxygen species), the most likely assignments for signal O2 is to superoxide radicals adsorbed on ceria sites affected in their environment by the presence of carbonate-type species, the presence of which is also demonstrated by FTIR (results not shown).

FTIR

Figure 5 shows the spectra in the carbonyl stretching region of Cu/CeO_2 following different treatments and CO adsorption experiments at different pressures. CO adsorption (10 Torr) on the initial calcined sample outgassed at RT (Fig. 5a) produces a main band at ca. 2100 cm^{-1}, with a shoulder at ca. 2115 cm^{-1} and minor bands in the 2185–2160 cm^{-1} range and at 2140 cm^{-1}. Both the band at 2100 cm^{-1} and the shoulder at 2115 cm^{-1} grow significantly upon increasing the CO pressure to 100 Torr; in this case a small band additionally appears at ca. 2057 cm^{-1} (Fig. 5b). Figure 5c shows the spectrum obtained after CO adsorption (10 Torr) on the sample reduced in CO and subsequently outgassed at $T_r = 373$ K, which presents mainly the band at 2100 cm^{-1} with a shoulder at ca. 2080 cm^{-1}; minor bands or shoulders are also observed at ca. 2160, 2115, 2057, and 2010 cm^{-1} (this latter being already present after the reduction treatment, prior to CO adsorption). When a higher CO pressure (100 Torr) is used (Fig. 5d), an intense shoulder at ca. 2115 cm^{-1} is produced while bands at 2050 and 2010 cm^{-1} grow; it is worth noting that in this case no significant intensity increase in the main band around 2100 cm^{-1} is apparently produced when increasing CO pressure, the spectrum showing a lower intensity than that found for similar CO pressure in the calcined sample (Fig. 5b). Subsequent thorough outgassing at RT (Fig. 5e) leads to the disappearance of the shoulders at 2115 and 2080 cm^{-1} while bands at 2100 and 2057 cm^{-1} retain most of their intensity and the band at 2010 cm^{-1} increases slightly.

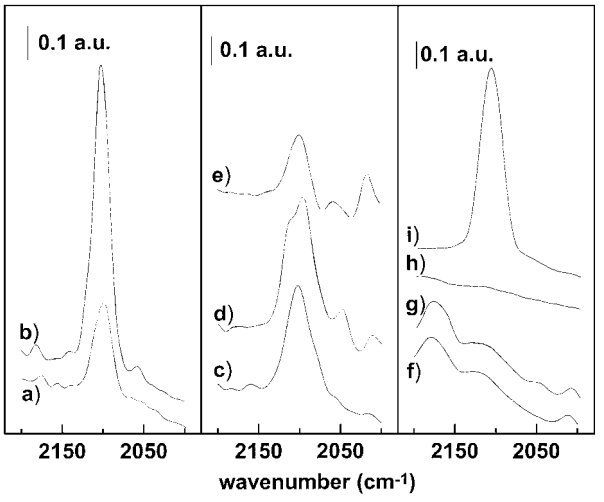

FIG. 5. FTIR spectra of Cu/CeO_2. Initial calcined sample exposed to CO at RT: (a) 10 Torr; (b) 100 Torr. Sample reduced in CO at $T_r = 373$ K exposed to CO at RT: (c) 10 Torr; (d) 100 Torr; (e) subsequent outgassing for 30 min at RT. (f) After reduction treatment in CO at $T_r = 473$ K; (g) subsequent adsorption of 100 Torr of CO at RT; (h) subsequent outgassing at RT and oxidation in 100 Torr of O_2; (i) subsequent outgassing at RT and exposure to CO (50 Torr) at RT.

The spectrum of the sample CO-reduced and then outgassed at $T_r = 473$ K shows, prior to CO adsorption, more or less broad bands at ca. 2180, 2120, and 2010 cm^{-1} (Fig. 5f). However, in contrast with the results obtained for lower T_r, almost no carbonyl band is observed (only a very small absorption increase is observed at ca. 2050 cm^{-1}; Fig. 5g) when up to 100 Torr of CO is adsorbed (the corresponding bands of CO(g) being clearly observed in the reference gas phase spectrum) or after subsequent RT outgassing. These results have shown to be reproducible when using other sample aliquots. Subsequent adsorption of O_2 at RT (Fig. 5h) eliminates almost completely all the bands in the 2200–2000 cm^{-1} range and, after outgassing at RT, a new CO adsorption produces an intense band at 2109 cm^{-1} (Fig. 5i). Results similar to those observed on the sample reduced at $T_r = 473$ K are obtained for Cu/CeO_2 treated at $T_r = 573$ K.

It is generally acknowledged that carbonyl bands at wavenumbers lower than about 2110 cm^{-1} are due to carbonyl species adsorbed on metallic copper particles (24), the variations in their wavenumbers being related to changes in the nature of the exposed metallic copper faces (i.e., on the coordination degree of the copper centers). In addition, it has to be considered that in the case of supported catalysts, metal–support interactions have been proposed (25, 26) to produce frequency shifts, with respect to the values obtained on unsupported metals. Other means of identifying the nature of the adsorption centers are based on the relative strengths of the CO–copper bonds; in this sense, considering species which could present overlapping frequencies, Cu^+ carbonyls show usually a significantly higher stability than Cu^0 carbonyls (27). Another aspect to consider concerns the extinction coefficients of the carbonyls, which are usually higher for Cu^+ carbonyls than for Cu^0 carbonyls (28).

On these bases, the feature appearing at ca. 2080 cm^{-1}, which is similar to bands of carbonyls formed on terrace sites of unsupported copper (24), can be attributed to carbonyl species adsorbed on metallic copper particles. Bands at 2058–2050 and 2010 cm^{-1}, showing a lower wavenumber, can also be tentatively assigned to Cu^0 carbonyls; their higher relative resistance towards outgassing at RT (Fig. 5e) is probably due to their location at copper–ceria interface sites, this in turn producing certain weakening of the C–O bond by interaction with the ceria support (29). A more thorough investigation, beyond the scope of this work, would certainly be needed to confirm these attributions. The feature at ca. 2115 cm^{-1}, which disappears upon RT outgassing, is most likely due to Cu^0 carbonyls adsorbed at defect sites of the metallic particles (24). Some doubts may exist regarding the nature of the adsorption center for the stronger bands observed at 2109–2100 cm^{-1}. Although Cu^0 carbonyls show bands in this range (24), an alternative assignment might be made on the basis of its ascription to Cu^+ sites and the existence of interactions of these with the underlying basic ceria support (14, 26, 29). Indeed, the higher resistance of this band towards RT outgassing strongly suggests that the corresponding bands are due to Cu^+ carbonyls.

Minor bands or shoulders at 2185–2160 cm^{-1} are most likely due to weakly adsorbed carbonyls on the ceria support (30) or on coordinatively unsaturated Cu^{2+} sites on CuO (31), while the weak bands observed at ca. 2140 cm^{-1} are probably due to Cu^+ carbonyls (25, 26). Considering their considerably lower intensity and poorer resolution in respect to the carbonyls mentioned in the previous paragraph, they will not be considered any further.

On the other hand, bands observed at 2180 and 2120 cm^{-1} in the spectrum of the sample reduced at $T_r = 473$ K (Fig. 5f) are probably due to purely electronic transitions in donor (Ce^{3+}) centers (29), although the band at 2120 cm^{-1} might also be due to highly stable Cu^+ carbonyls (25–27). The first hypothesis is supported by experiments performed on the Cu-free support (data not shown), which showed bands at 2185 and 2127 cm^{-1} after reduction treatment in CO and subsequent outgassing at $T_r = 573$ K.

TABLE 2

XPS Data for the Initial Calcined Cu/CeO_2 Sample: Cu $2p_{3/2}$ and Ce $3d_{5/2}$ Binding Energies (eV), Cu LMM Auger Parameter α (eV), Intensity of the Ce^{4+} Satellite at ca. 916 eV (Expressed as Percentage of Total Ce Peak Intensity), and Cu/Ce Atomic Ratio

Cu $2p_{3/2}$	α	Ce $3d_{5/2}$	Ce^{4+} sat. (%)	$(Cu/Ce)_{at}$
933.8 (80%) 935.4 (20%)	1851.4	881.9	12	0.048

XPS

XPS data for an *in situ* calcined Cu/CeO_2 aliquot are reported in Table 2. For cerium, the position of the $3d_{5/2}$ XPS peak, as well as the intensity of the satellite peak at BE $\approx$ 916 eV, agrees well with a fully oxidized Ce^{4+} state. For copper, a relatively broad and asymmetric main Cu $2p_{3/2}$ line centered at BE $\approx$ 934.5 eV has been observed, which can be due to the contribution of different copper species. Satisfactory simulation of the XPS peak is achieved by considering the contribution of two components at 935.4 and 933.8 eV, the latter being the dominant one. A survey of literature data (Table 3) points out the difficulty in the unambiguous attribution of the copper nature on an XPS-only basis, particularly in cases when the copper phase is highly dispersed and in intimate contact with supports, as it occurs for Cu ions in zeolites or for small Cu^0 particles supported on reducible oxides such as TiO_2. However, in the present case, the spectrum of the calcined material displays a relatively large satellite peak (showing ca. 25% of the intensity of the main peak) centered at ca. 941.5 eV BE; furthermore, the position of the Cu_{LMM} Auger peak detected, combined with that of the dominant Cu $2p_{3/2}$ contribution, yields for

TABLE 3

Representative Values of Cu $2p_{3/2}$ Level Binding Energy (eV) and Cu LMM Auger Parameter α (eV), Reported in the Literature for Copper Species in Several Well-Defined Materials

Cu species (sample)	Cu $2p_{3/2}$ BE	α	References
Cu^{2+} (CuO)	933.8	1851.0	32
Cu^+ (Cu_2O)	932.5	1849.6	32
Cu^{2+} ions (exchanged in zeolites)	935.2	1849.5	34
Cu^+ ions (exchanged in zeolites)	933.8	1847.2	34
Cu^0/TiO_2 (7×10^{13} atoms cm^{-2})	933.1	1847.9	35
Cu^0/TiO_2 ($\approx$14 Å thick Cu layer)	932.7	1851.5	35

the latter an Auger parameter value $\alpha = 1851.4$ eV. Based on both observations, the main XPS contribution can be safely ascribed to a CuO-like phase, (32, 33).

The minority component (at 935.4 eV BE; its Auger peak cannot be resolved) of the oxidized material might be attributed to isolated Cu^{2+} ions, similar to those observed in Cu^{2+}-exchanged zeolites (34).

DISCUSSION

Initial State of Copper

Several questions were raised in a previous preliminary work on this Cu/CeO_2 sample (11), concerning the nature of the copper species present in the initial calcined sample. Since only ca. 25% of the copper present is well characterized as forming different Cu^{2+} species on the basis of EPR experiments, and a significant amount of carbonyls adsorbed on reduced copper centers is observed by FTIR after CO adsorption at RT, an immediate interpretation to account for the remaining EPR-silent ca. 75% of the copper was the stabilization by ceria, already in the calcined state of the sample, of diamagnetic Cu^{+}-type species, as proposed in previous reports on coprecipitated Cu–Ce oxide samples (10). However, XPS data reported in this work strongly suggest that most of the copper is initially in a fully oxidized Cu^{2+} state. This result is in agreement with a previous report on Cu–Ce oxide catalysts (36), in which, based on XPS data, no evidence of the presence of Cu^{+} ions stabilized by interactions with cerium oxide was found for preoxidized materials. Thus, as expected considering the oxidative pretreatment of the sample, and according to the XPS results reported here, most of the copper (75–80%) in Cu/CeO_2 is present as Cu^{2+} species in a CuO-like phase (contribution at BE = 933.8 eV). These are not detected by EPR due to strong magnetic interactions, known to be antiferromagnetic (37), between Cu^{2+} ions in this phase; other interpretations based on symmetry or weak Cu–Cu coupling effects, leading to EPR-nondetectable dispersed paramagnetic Cu^{2+} ions (as observed in some cases in Cu-exchanged zeolites (38)), seem less likely in view of the good correlation observed between the amount of Cu^{2+} ions detected by EPR and the intensity of the XPS line at 935.4 eV ascribed to dispersed Cu^{2+}. These results indicate that ca. 20–25% of the copper is more or less well dispersed on the ceria support forming Cu^{2+} species, the main part of this fraction being present as isolated entities (signals type C), while a smaller part is forming Cu^{2+}–Cu^{2+} ionic pairs (signal K) and other Cu^{2+} ions are located in somewhat more aggregated CuO clusters (signal B).

Effect of CO on the Redox State of Copper

Copper reduction by interaction with CO is produced already at RT, as revealed by results of the different techniques employed, the intensity decrease in the Cu^{2+} signals detected by EPR (Fig. 2) being the strongest evidence of the occurrence of this process. Analysis of the evolution of the different EPR signals when the sample is subjected to reduction treatments in CO shows that isolated Cu^{2+} species type C (signals), particularly those with a higher degree of coordinative unsaturation (signal C2), are more reducible than copper ionic pairs (signal K) and these, in turn, more than CuO clusters (signal B), suggesting that the Cu^{2+} reducibility with CO at low temperature decreases with its aggregation degree.

It should be noted, however, that a very small part of the isolated Cu^{2+} species is stable even after reduction at $T_r \geq 473$ K (signal C3), which has been attributed to the location of these sites at subsurface positions, stabilized by the ceria lattice.

Considering that the initial calcined sample presents copper mainly in a fully oxidized state, the formation of Cu^{+} carbonyls and, to a lower degree, Cu^{0} carbonyls by contacting the sample with CO at RT (Figs. 5a and 5b) indicates that CO interacts with Cu^{2+} ions with unsaturated coordination, originating their reduction with formation of CO_2; a subsequent CO adsorption on the reduced centers produces the carbonyl species. Correlation of this result with the CO consumption peak observed at RT in the TPR experiment (Fig. 1) and the fact that no CO_2 evolution is produced at that T_r indicates that the generated CO_2 remains chemisorbed on the sample (probably forming carbonate species adsorbed on the ceria support (30); a large absorbance is observed in all cases in the carbonate region of the FTIR spectra, disallowing a detailed analysis of the species formed).

The higher IR extinction coefficients of Cu^{+} carbonyls with respect to Cu^{0} carbonyls (28) suggest, when comparing the FTIR spectra of Figs. 5b and 5d, that Cu^{+} species could predominate for T_r = RT, while a higher amount of Cu^{0} could be present for $T_r = 373$ K. Formation of carbonyls at terrace sites of metallic copper particles (feature at ca. 2080 cm^{-1}), which were absent or presented a significantly lower intensity on the sample reduced at T_r = RT, further supports the formation of relatively larger metallic copper particles at $T_r = 373$ K. Achievement of a higher copper reduction degree after treatment at $T_r = 373$ K is also supported by the EPR results (Fig. 2) showing a significant decrease in the intensity of Cu^{2+} signals at that T_r.

A remarkable observation here is that only a very small amount of carbonyls are formed upon CO adsorption on the sample reduced at $T_r \geq 473$ K (Figs. 5f and 5g). Although complete copper reduction (to metallic copper) and further copper sintering could produce significant decreases in the amount of copper carbonyls detected (14, 39, 40), and CO adsorbs normally more weakly on Cu^{0} than on Cu^{+} (24–28), this alone is not likely to explain the result obtained, since well-developed IR bands of Cu^{0} carbonyls are usually observed on other copper-containing catalysts using the same

equilibrium pressures used here (24, 27), and further, these carbonyls are clearly detected on the Cu/CeO_2 sample reduced at $T_r = 373$ K. The results outlined above point rather to the onset of some kind of strong metal–support interaction, by which metallic copper loses its capacity to adsorb carbon monoxide upon treatment in CO at $T_r \geq 473$ K. Similar arguments have been used to explain the significant decrease in the metallic copper carbonyls produced upon CO adsorption at RT on Cu/TiO_2 submitted to reduction in H_2 at relatively high temperatures (40). Decoration of the copper particles by titanium suboxides was invoked in that case to account for the observed results, and indeed some encapsulation effect of copper by ceria upon reduction with H_2 of $Cu/CeO_2/Al_2O_3$ catalysts was shown by XPS/sputtering experiments (33). In our case this is not likely to be the dominant effect, since the CO adsorption capability is recovered simply by copper reoxidation upon O_2 contact at RT, while recovery of the adsorption capability in particles affected by support decoration usually requires significantly higher reoxidation temperatures (41). A possible interpretation could be the presence of electronic interactions between small metallic copper particles and reduced ceria. The driving force for this metal–support interaction could be the achievement of a relatively strong reduction of the ceria surface by treatment at $T_r > 373$ K. The relatively large CO consumption level achieved at those T_r in the TPR experiment (Fig. 1) supports this interpretation. Electron transfer from Ce^{3+} towards the Cu particles could then produce a Cu–CO interaction even weaker than on neutral Cu^0, leading to a depletion in the amount of adsorbed CO in the conditions of our IR experiments. Other possible effects involving plasmon absorption processes (which could produce decreases in the number of adsorbed entities detected by infrared (29)) might also contribute to the almost full depletion in the detected carbonyl species, though observation of both hydroxyl and carbonate-related species under the experimental conditions of the spectrum of Fig. 5g suggests this effect is not strong in the present case.

Reoxidation of the Copper Species

Reoxidation of copper in the CO-reduced sample by contact with O_2 is already produced at RT, as demonstrated by the increase in the intensity of Cu^{2+} signals revealed by EPR (Fig. 4) and by the formation of Cu^+ carbonyls shown by FTIR (Fig. 5i). Overall, the reoxidation treatment seems to lead to a more homogeneous situation than that present in the initial calcined state, on the basis of the formation of a single symmetric band in the FTIR spectrum following CO adsorption on the sample reoxidized at RT (Fig. 5i) and the uncompleted recovery of the intensity of the initial EPR spectrum (Fig. 2a) after reoxidation treatments (Fig. 4). This may be due to an effect of copper redistribution produced during the reduction treatments in CO, leading at the end to a higher relative amount of less dispersed EPR-silent CuO-type species in the reoxidized sample than in the initial sample. Stabilization of Cu^+ species after the redox cycle could also partially explain these observations.

According to the EPR results, copper reoxidation affects first copper ions placed at subsurface ceria locations (giving rise to signal C3). Paired and clustered copper (yielding signals K and B, respectively) are also reoxidized at RT upon contact with a larger amount of O_2, while isolated copper species exposed at the ceria surface require heating at 473 K, thus showing a trend opposite that shown upon reduction, which revealed these latter (signals C1 and C2) were the most reducible. The easier reoxidation of species C3, with respect to the exposed Cu^{2+} species, indicates a promoting effect of ceria: since those isolated Cu^{2+} species are stabilized by ceria at subsurface positions, the strong reoxidation of the ceria surface produced by O_2 interaction at RT, as discussed below, could induce the reoxidation of these particular Cu^{2+} centers.

Effects of CO Reduction and O_2 Adsorption on the Ceria Support

As revealed by the EPR data obtained after O_2 adsorption on the reduced Cu/CeO_2 sample, CO has reducing effects at RT also on the ceria component. The formation of Ce^{4+}–O_2^- entities upon O_2 adsorption at 77 K or RT on the sample reduced at $T_r \geq$ RT, which would follow the process Ce^{3+}–$V_o + O_2 \rightarrow Ce^{4+}$–$O_2^-$ (21) (where V_o denotes a doubly ionized oxygen vacancy), clearly indicates that reduced cerium cations had been generated by the reduction pretreatment.

On the other hand, the decrease (or disappearance) of superoxide entities observed upon warming at RT the sample with O_2 adsorbed at 77 K, which is more pronounced when relatively low O_2 doses are adsorbed, cannot be attributed to copper reoxidation since the effect has been observed in cases when the amount of oxygen admitted in the cell is considerably larger than that theoretically required for a complete reoxidation of copper (280 μmol g^{-1} of O_2 adsorbed vs 157 μmol g^{-1} of copper). The most plausible hypothesis to account for these observations is the formation of (diamagnetic) O_2^{2-} (peroxide anions) or O^{2-} (oxide anions) entities (which would require transfer of two or more electrons per O_2 molecule adsorbed) as a consequence of the O_2 interaction with the CO-reduced ceria surface. The ceria subsurface reoxidation, revealed by the increase of signal C3 upon oxygen contact, indicates that the most likely reoxidation mechanism follows O_2 dissociation and formation of oxide anions. When a decrease of the reductive power of ceria is achieved after a certain surface reoxidation degree is attained by O_2 predosing, superoxide entities (requiring transfer of only one electron per oxygen molecule) are more easily stabilized. The absence of these effects in previous works (17–20), in which ceria-related systems were submitted to vacuum reduction prior to oxygen

adsorption, would then be explained by the lower ceria reduction degree attained in those cases. Similar behavior upon interaction with O_2 is observed for the copper-free ceria support reduced in CO at $T_r > 473$ K, suggesting that copper might not be involved in a promoting effect on ceria reoxidation; its role would be mainly related to the strong promotion of ceria reduction, and indeed these effects are observed in the presence of copper at rather lower T_r, while pure ceria only achieves such a more deeply reduced state at $T_r > 473$ K, in agreement with magnetic susceptibility measurements on other CO-reduced ceria samples (42).

The fact that signals O2, rather than signal O1, appear after adsorption on deeply reduced ceria of relatively high amounts of O_2 at RT suggests that the Ce^{3+} species with a more moderate tendency to reoxidation are those affected by the presence of carbonate species in their coordination environment. Reduced ceria zones at which carbonate species are not stabilized show a higher reducing power, as follows from the fact that species giving rise to signal O1, attributed to superoxide species formed on ceria centers less affected by the presence of carbonate complexes, are the first ones to be formed by O_2 adsorption at 77 K and are also the most easily destroyed upon warming at RT. This indicates that the most reactive zones for ceria reoxidation are those present at sites free of carbonate influence.

Redox Synergy between Cu and CeO_2

Finally, it is worth noting the significantly higher redox capacity of this Cu/CeO_2 system, in comparison to other supported copper systems like Cu/Al_2O_3. For this latter, a very small copper reduction level is achieved by interaction at RT and no important copper reduction is produced until $T_r \geq 573$ K (11, 14). Although in that case, interactions between copper and alumina leading to formation of surface Cu–Al spinel phases could play an important role in stabilizing copper against complete reduction to Cu^0 (33, 39), comparison with unsupported CuO, in which a very small copper reduction is also produced by interaction with CO at RT (25), reveals that a promoting effect is produced in the reduction of copper, induced by its interaction with the ceria support. Similarly, comparison with the copper-free support shows that ceria reduction is also strongly enhanced by the influence of copper. In view of the results obtained, it has to be considered that the promoting effect for CO catalytic oxidation observed upon establishment of contacts between copper and cerium oxide (10, 11) could involve redox processes by which both copper and ceria are simultaneously reduced and oxidized in a cooperative process.

CONCLUSIONS

—XPS results indicate that copper entities are in a fully oxidized Cu^{2+} oxidation state for the initial calcined Cu/CeO_2 sample. On the basis of EPR and XPS experiments, ca. 25% is forming more or less dispersed species, while ca. 75% is forming a CuO-like phase which escapes EPR detection.

—Cu^{2+} species are reduced by CO even at RT in the Cu/CeO_2 catalyst. EPR results suggest in general terms that the reducibility of Cu^{2+} decreases with its aggregation degree.

—After reduction with CO at $T_r \geq 473$ K, the CO adsorption capability of copper is very strongly diminished. This effect is attributed to the onset of strong electronic interactions between reduced ceria and small metallic copper particles generated by the reduction treatment, and is reversed by mild reoxidation induced by simple contact with O_2 at RT.

—Ceria reduction by CO is produced at $T_r \geq$ RT, being strongly promoted by copper. Reduced zones at the ceria surface both free and affected by the presence of carbonate complexes are observed to be formed in Cu/CeO_2 by the reduction process, the first of them showing significantly higher reactivity towards O_2.

—In general terms, a remarkable redox activity is shown by this Cu/CeO_2 catalyst, reduction/oxidation processes of both copper and ceria being observed at temperatures as low as RT. This significant redox activity is thought to be of crucial importance in explaining the remarkably high CO oxidation rates observed for this system (11).

ACKNOWLEDGMENTS

Financial help from CICYT (Project MAT97-0696-C02-01) and the Comunidad de Madrid (Project 06M/085/96) is acknowledged. Thanks are due to Professor J. L. G. Fierro and Mr. E. Pardo for obtaining the XPS data. A. M.-A. and M. F.-G. acknowledge the Comunidad Autónoma de Madrid and the CSIC, respectively, for postdoctoral grants under which this work has been carried out.

REFERENCES

1. Trovarelli, A., *Catal. Rev. Sci. Eng.* **38**, 439 (1996).
2. (a) Dictor, R., and Roberts, S., *J. Phys. Chem.* **93**, 5846 (1989). (b) Su, E. C., and Rothschild, W. G., *J. Catal.* **99**, 506 (1986).
3. (a) Yao, H. C., and Yu Yao, Y. F., *J. Catal.* **86**, 254 (1984). (b) Engler, B., Koberstein, E., and Schubert, P., *Appl. Catal.* **48**, 71 (1989). (c) Miki, T., Ogawa, T., Haneda, M., Kakuta, N., Ueno, A., Tateishi, S., Matsuura, S., and Sato, M., *J. Phys. Chem.* **94**, 6464 (1990).
4. (a) Shido, T., and Iwasawa, Y., *J. Catal.* **136**, 493 (1992). (b) Shido, T., and Iwasawa, Y., *J. Catal.* **141**, 71 (1993).
5. Martínez-Arias, A., Soria, J., Conesa, J. C., Seoane, X. L., Arcoya, A., and Cataluña, R., *J. Chem. Soc. Faraday Trans.* **91**, 1679 (1995).
6. Hardacre, C., Ormerod, R. M., and Lambert, R. M., *J. Phys. Chem.* **98**, 10901 (1994).
7. (a) Zafiris, G. S., and Gorte., R. J., *J. Catal.* **139**, 561 (1993). (b) Cordatos, H., Ford, D., and Gorte, R. J., *J. Phys. Chem.* **100**, 18128 (1996).
8. Martínez-Arias, A., Soria, J., and Conesa, J. C., *J. Catal.* **168**, 364 (1997).
9. Shaw, E. A., Rayment, T., Walker, A. P., and Lambert, R. M., *Appl. Catal.* **67**, 151 (1990).

10. (a) Liu, W., Sarofim, A. F., and Flytzani-Stephanopoulos, M., *Chem. Eng. Sci.* **49**, 4871 (1995). (b) Liu, W., and Flytzani-Stephanopoulos, M., *J. Catal.* **153**, 304 (1995).
11. Martínez-Arias, A., Soria, J., Cataluña, R., Conesa, J. C., and Cortés Corberán, V., *Stud. Surf. Sci. Catal.* **116**, 591 (1998).
12. Park, P. W., and Ledford, J. S., *Catal. Lett.* **50**, 41 (1998).
13. Luo, M.-F., Zhong, Y.-J., Yuan, X.-X., and Zheng, X.-M., *Appl. Catal. A* **162**, 121 (1997).
14. Martínez-Arias, A., Cataluña, R., Conesa, J. C., and Soria, J., *J. Phys. Chem. B* **102**, 809 (1998).
15. Jernigan, G. G., and Somorjai, G. A., *J. Catal.* **147**, 567 (1994).
16. (a) Abou Kaïs, A., Bennani, A., Aïssi, C. F., Wrobel, G., Guelton, M., and Védrine, J., *J. Chem. Soc. Faraday Trans.* **88**, 615 (1992). (b) Abou Kaïs, A., Bennani, A., Aïssi, C. F., Wrobel, G., and Guelton, M., *J. Chem. Soc. Faraday Trans.* **88**, 1321 (1992). (c) Soria, J., Conesa, J. C., Martínez-Arias, A., and Coronado, J. M., *Solid State Ionics* **63–65**, 755 (1993).
17. Kucherov, A. V., Slinkin, A. A., Kondratev, D. A., Bondarenko, T. N., Rubinstein, A. M., and Minachev, K. M., *Zeolites* **5**, 320 (1985).
18. Aboukaïs, A., Bechara, R., Ghoussoub, D., Aïssi, C. F., Guelton, M., and Bonnelle, J. P., *J. Chem. Soc. Faraday Trans.* **87**, 631 (1991).
19. Soria, J., Martínez-Arias, A., and Conesa, J. C., *J. Chem. Soc. Faraday Trans.* **91**, 1669 (1995).
20. Soria, J., Coronado, J. M., and Conesa, J. C., *J. Chem. Soc. Faraday Trans.* **92**, 1619 (1996).
21. Martínez-Arias, A., Coronado, J. M., Conesa, J. C., and Soria, J., *in* "Rare Earths" (R. Sáez Puche and P. Caro, Eds.), p. 299, Editorial Complutense, Madrid, 1997.
22. Soria, J., Conesa, J. C., and Martínez-Arias, A., *Coll. Surf. A*, in press.
23. Rojo, J. M., Sanz, J., Soria, J., and Fierro, J. L. G., *Z. Phys. Chem.* **152**, 149 (1987).
24. Hollins, P., *Surf. Sci. Rep.* **16**, 51 (1992).
25. Lokhov, Y. A., Sadykov, V. A., Tikhov, S. F., and Popovskii, V. V., *Kinet. Katal.* **26**, 177 (1985).
26. Davydov, A. A., *Kinet. Katal.* **26**, 157 (1985).
27. Padley, M. B., Rochester, C. H., Hutchings, G. J., and King, F., *J. Catal.* **148**, 438 (1994).
28. Kohler, M. A., Cant, N. W., Wainwright, M. S., and Trimm, D. L., *J. Catal.* **117**, 188 (1989).
29. Bensalem, A., Muller, J.-C., Tessier, D., and Bozon-Verduraz, F., *J. Chem. Soc. Faraday Trans.* **92**, 3233 (1996).
30. Li, C., Sakata, Y., Arai, T., Domen, K., Maruya, K., and Onishi, T., *J. Chem. Soc. Faraday Trans. 1* **85**, 929 (1989).
31. Busca, G., *J. Mol. Catal.* **43**, 225 (1987).
32. "Handbook of X-ray Photoelectron Spectroscopy." Perkin–Elmer, New York, 1978.
33. Fernández-García, M., Gómez Rebollo, E., Guerrero Ruiz, A., Conesa, J. C., and Soria, J., *J. Catal.* **172**, 146 (1977).
34. Grunet, W., Hayes, N. W., Joyner, R. W., Shpiro, E. S., Siddiqui, M. R. H., and Baera, G. N., *J. Phys. Chem.* **42**, 10832 (1992).
35. Carley, A. F., Rajumon, M. K., and Roberts, M. W., *J. Solid State Chem.* **106**, 156 (1993).
36. Lamonier, C., Bennani, A., D'Huysser, A., Aboukaïs, A., and Wrobel, G., *J. Chem. Soc. Faraday Trans.* **92**, 131 (1996).
37. Mehran, F., Barnes, S. E., Chandrashekhar, G. V., Mc Guire, T. R., and Shafer, M. W., *Solid State Commun.* **67**, 1187 (1988).
38. (a) Conesa, J. C., and Soria, J., *J. Phys. Chem.* **82**, 1847 (1978). (b) Lo Jacono, M., Fierro, G., Dragone, R., Feng, X., d'Itri, J., and Hall, W. K., *J. Phys. Chem. B* **101**, 1979 (1997).
39. Sepúlveda, A., Márquez, C., Rodríguez-Ramos, I., Guerrero-Ruiz, A., and Fierro, J. L. G., *Surf. Interface Anal.* **20**, 1067 (1993).
40. Boccuzzi, F., Chiorino, A., Martra, G., Gargano, M., Ravasio, N., and Carrozzini, B., *J. Catal.* **165**, 129 (1997).
41. Belzunegui, J. P., Sanz, J., and Rojo, J. M., *J. Am. Chem. Soc.* **114**, 6749 (1992).
42. Badri, A., Lamotte, J., Lavalley, J. C., Laachir, A., Perrichon, V., Touret, O., Sauvion, G. N., and Quemere, E., *Eur. J. Solid State Inorg. Chem.* **28**, 445 (1991).